Inverse calculation of biochemical oxygen demand models based on time domain for the tidal Foshan River

Li Er and Zeng Xiangying

ABSTRACT

To simulate the variation of biochemical oxygen demand (BOD) in the tidal Foshan River, inverse calculations based on time domain are applied to the longitudinal dispersion coefficient (E(x)) and BOD decay rate (K(x)) in the BOD model for the tidal Foshan River. The derivatives of the inverse calculation have been respectively established on the basis of different flow directions in the tidal river. The results of this paper indicate that the calculated values of BOD based on the inverse calculation developed for the tidal Foshan River match the measured ones well. According to the calibration and verification of the inversely calculated BOD models, K(x) is more sensitive to the models than E(x) and different data sets of E(x) and K(x) hardly affect the precision of the models.

Key words | BOD decay rate, inverse calculation, longitudinal dispersion coefficient, time domain

Li Er (corresponding author)
Zeng Xiangying
Wuhan Municipal Engineering Design and Research Institute,
Changqing Road 40, Jianghan District,
Wuhan 430015,
China
E-mail: *tjy903@163.com*

INTRODUCTION

In recent years, concerns have grown on the pollution of the tidal river in China. Tides are the periodic rise and fall of the sea level due to attractive forces of the sun, moon, and earth. Tides and tidal currents are a major source of energy for turbulence and mixing in estuaries and they play an important role in the movement of dissolved and particulate material, creating oscillatory fluxes in physical and chemical properties. The dissipation of tidal energy causes changes in the vertical stability of the water column. Denman & Powell (1984) showed that tidal mixing is important for phytoplankton and primary productivity because it produces light and nutrient fluctuations. Yin *et al.* (1995) showed that the tidal-regulated estuarine circulation played an important role in entrainment of nutrients in the Fraser River estuary and adjacent coastal waters of the Strait of Georgia (Canada). Compared with a non-tidal river, pollutants in a tidal river distribute uniformly throughout the whole cross-sections more rapidly. Therefore a one-dimensional water quality model can be fit for a tidal river (Atkinson *et al.* 2009; Ghermandi *et al.* 2009; Franceschini & Tsai 2010; Mannina & Viviani 2010). Biochemical oxygen demand (BOD) is a crucial index indicating organic pollution status of water, and the study of BOD models for rivers is growing (Ani *et al.* 2009; Telci *et al.* 2009; Erturk *et al.* 2010). As crucial parameters, longitudinal dispersion coefficient (E(x)) and BOD decay rate (K(x)) of one-dimensional water quality models for BOD vary with different downstream distance of a tidal river (Wagener *et al.* 2001). Inverse calculation is an effect mathematical method to develop a tidal river's BOD model (Paredes *et al.* 2010; Freni *et al.* 2011), for it has such characteristics as high efficiency and accuracy in turning infinite variables into finite equations, and fast transformation of the corresponding initial and boundary conditions of the equations into finite constrained ones (Beck *et al.* 1996; Zheng & Gore 2005).

The objective of this paper is to establish the inverse calculation of the BOD model on the basis of E(x) and K(x) for the tidal Foshan River in China. As a feature, the increasing number of the distributed parameters in an inverse calculated model tends to lead to the occurrence of ill-conditioned equations (Zheng & Gore 2005; Erturk *et al.* 2010). In addition multi-parameter inverse calculation equations cause high nonlinear problems very easily (Beck *et al.* 1996). Therefore the conventional optimal parameters estimation methods such as discrete optimizing theory and pulse-spectrum technique are not fit for inversely calculated BOD models, and the compound approach in which inverse calculation developed based on time domain is in effect (Beck *et al.* 1996; Zheng & Gore 2005). The inverse calculation of BOD models in time domain for the tidal Foshan River is calibrated and verified in this work.

doi: 10.2166/wst.2014.177

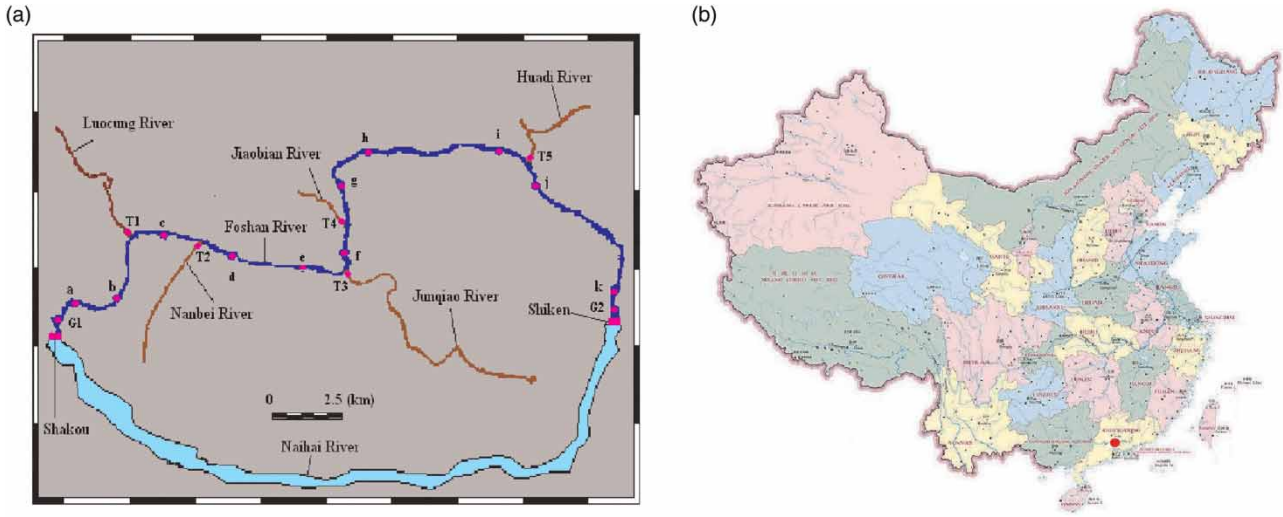

Figure 1 | (a) Profile map of the tidal Foshan River including location of stations and (b) location of the tidal Foshan River (circle).

PROFILE OF THE FOSHAN RIVER

The tidal Foshan River, connected with the tidal Nanhai River on its western and eastern estuary, is situated in southern China (shown in Figure 1). The width of the river ranges from 0.3 to 0.8 km and the length of it is about 28.5 km. The tide of this river mainly comes from the Pacific Oceanic tidal propagation through the Dongping Strait with a mean tidal range between 1.0 and 1.7 m, and also affected by the geometry and bottom topography, and meteorological factors (Er *et al.* 2009; Svejkovsky *et al.* 2010). There have been large-scale field observations and research on tides and tidal flows in the tidal Foshan River in the past, from which it can be concluded that the tidal cycle in this area is mainly a semi-diurnal mixed tidal regime with daily inequality in range and time between the period of high flows and low flows. In addition the water level of the Nanhai River influences the tide of the tidal Foshan River. When its water level is less than 1.0 m, the tide appears considerably strong, and when its water level exceeds 1.7 m the tide becomes quite weak. The pattern of residual flows in the tidal Foshan River reciprocates owing to the different tidal force between its western and eastern part (Er *et al.* 2009; Svejkovsky *et al.* 2010).

Hydrological monitoring and water quality monitoring stations were distributed in the whole river and its tributaries. The stations a–k (called Stn a–k for short) and the stations T1–T5 (called Stn T1–T5 for short) were set up in the main river and its tributaries for measuring their respective BOD (ultimate carbonaceous BOD ($CBOD_u$)), flow rate and flow velocity, and the stations G1–G2 (called Stn G1–G2 for short) were established in the estuary of the main river for measuring its tidal indices. Field measurements of Stn a–k and T1–T5 were obtained during cruises in March, April, June, July, September, October, November and December in 2012, and those of Stn G1–G2 were got in the whole of 2012. Flow velocity and flow direction at all the stations were consecutively recorded with a Nortek ADP-1500 mounted on the sediment bottom. The values of BOD were measured based on the standardized procedure (Ani *et al.* 2009; Xiangying *et al.* 2012).

MODEL

One-dimensional BOD models for the tidal Foshan River

The BOD model of the tidal Foshan River may be consecutively established on a reach by reach basis. According to the measurements of each sampling station, the maximum BOD and flow rates from the tributaries of the river are shown in Figure 2. The ranges of the ratio of the flow rate and total BOD of the tributaries to the main river were measured

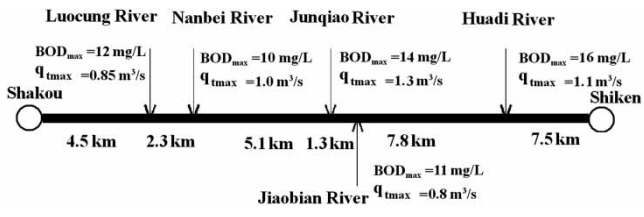

Figure 2 | BOD and flow rate contributed from tributaries of the tidal Foshan River. BOD_{max} is the maximum BOD of each tributary during the measurement period; q_{max} is the maximum flow rate of each tributary during the measurement period.

as follows: 0.16–2.03% and 0.15–0.72% in the Luocung River, 0.21–1.93% and 0.11–0.65% in the Nanbei River, 1.1–3.21% and 0.8–1.6% in the Junqiao River, 0.22–1.88% and 0.17–0.61% in the Jiaobian River, and 0.23–2.28% and 0.26–0.79% in the Huadi River respectively.

Therefore, it can be concluded that the flow rate and total BOD of the main stream are more than those from each tributary. And past measurements have shown that the total BOD from other potential pollution sources along tributaries contribute little to the main stream based on past measured (Xiangying *et al.* 2012). Therefore under unsteady flow conditions, the one-dimensional BOD model together with its initial and boundary conditions, ignoring the component caused by other potential pollution sources and tributaries (Ghermandi *et al.* 2009), can be developed as follows:

$$\begin{cases} \dfrac{\partial C(x,t)}{\partial t} + u\dfrac{\partial C(x,t)}{\partial x} = \dfrac{\partial}{\partial x}\left[E(x)\dfrac{\partial C(x,t)}{\partial x}\right] - K(x)\cdot C(x,t) \\ C(0,t) = f(t)C(l,t) = g(t)t \in [0,T]C(x,0) \\ \qquad = \varphi(x)x \in [0,l]\dfrac{\partial C(x,t)}{\partial x}\Big|_{x=l} = 0t \in [0,T] \end{cases} \tag{1}$$

where x is stream distance (L), t is stream time (T), u is cross-sectional flow velocity (LT^{-1}), $C(x,t)$ is concentration of $CBOD_u$ (ML^{-3}) at a distance x(L) downstream at a time t(T), $E(x)$ is longitudinal dispersion coefficient (L^2T^{-1}), $K(x)$ is BOD decay rate at a distance x (T^{-1}), T is the whole time of the stream time (T), $\partial/\partial t$ is partial differential expression of t, $\partial/\partial x$ is partial differential expression of x, l is whole length of the river (L), $f(t)g(t)$ is the function of t and $\varphi(x)$ is the function of x.

The inverse calculation based on time domain in different flow direction

The flow direction of a tidal river

A tidal river can be divided into many reaches and there are four types of flow directions existing in each reach in a tidal river during a tide: forward flow, backward flow, divergent flow and convergent flow. In this paper, the flow directions from a reach's western side to its eastern side and from a reach's eastern side are respectively called as 'forward flow' and 'backward flow'. The flow directions from a reach's centre to its two sides and from both sides of a reach to its centre are respectively defined as 'divergent flow' and 'convergent flow'. Both 'forward flow' and 'backward flow' are called as 'unidirectional flow', and both 'divergent flow' and 'convergent flow' are named as 'multidirectional flow'. Obviously there are three directions in ('forward flow', 'backward flow' and 'multidirectional flow') all reaches of a tidal river at the same time, and the BOD model of a tidal should be developed in these respective directions.

The inverse calculation models based on time domain

Under the forward flow direction condition, the numerical solution of Equation (1), together with its initial and boundary conditions, is obtained by discretizing it over a non-uniform rectangular grid and the corresponding unconditional stable implicit finite difference scheme as follows:

$$\begin{cases} \dfrac{C_{i,j+1}-C_{i,j}}{\tau} + u\dfrac{C_{i+1,j+1}-C_{i,j+1}}{h} \\ \quad = \dfrac{E_{i+1}C_{i+1,j+1} - (E_{i+1}+E_i)C_{i,j+1} + E_iC_{i-1,j+1}}{h^2} - K_iC_{i,j+1} \\ C_{0,j} = f(j\tau),\ C_{i,0} = \varphi(ih),\ C_{N+1,j} = C_{N,j},\ C_{N,j} = g(j\tau) \\ C_{i,j}^{n+1} = C_{i,j}^n + \delta C_{i,j}^n,\ E_i^{n+1} = E_i^n + \delta E_i^n,\ K_i^{n+1} = K_i^n + \delta K_i^n \\ (i = 0, 1, 2, \ldots N, j = 0, 1, 2, \ldots W) \end{cases} \tag{2}$$

where τ is the time step (T), h is the distance step (L), and $C_{i,j}^n$, E_i^n and K_i^n represent the nth iterative value of $C(x_i, t_j)$, $E(x_i)$ and $K(x_i)$ in the ith reach respectively. x_i is the ith spatial grid stream distance, t_j is the ith grid time, $\delta C_{i,j}^n$ is the difference between $C_{i,j}^n$ and $C_{i,j}^{n+1}$, δE_i^n is the difference between E_i^{n+1} and E_i^n, and δK_i^n is the difference between K_i^{n+1} and K_i^n.

The transition matrix M of Equation (2) is expressed as follows:

$$M = \frac{(1-\mu+\mu\cos Kh) - i\dfrac{\lambda}{2}\sin Kh}{(1+\mu-\mu\cos Kh+K\tau) + i\dfrac{\lambda}{2}\sin Kh} \tag{2a}$$

where $\lambda = u(\tau/h)$, $\mu = (\tau/3h^2)(E_{i-1}+E_i+E_{i+1})$, and the determinant of the matrix M is the following expression:

$$|M|^2 = \frac{(1-\mu+\mu\cos Kh)^2 - \left(\dfrac{\lambda}{2}\sin Kh\right)^2}{(1+\mu-\mu\cos Kh+K\tau)^2 + \left(\dfrac{\lambda}{2}\sin Kh\right)^2} \tag{2b}$$

According to Equation (2b), the following equation is obtained:

$$|M|^2-1=\frac{-8\mu\sin^2 Kh-K\tau(2+4\mu\sin^2 Kh+K\tau)}{(1+\mu-\mu\cos Kh+K\tau)^2+\left(\frac{\lambda}{2}\sin Kh\right)^2} \tag{2c}$$

Obviously, $|M|^2-1\le 0$, therefore $|M|^2\le 1$. So based on the equivalence theorem, Equation (2) is a convergence equation.

According to Equation (2), the expression of the forward calculation model about $C_{i,j}^n$ and its initial and boundary conditions can be yielded as follows:

$$\begin{cases}\left(\frac{u}{h}-\frac{E_{i+1}^n}{h^2}\right)C_{i+1,j+1}^n+\left(\frac{1}{\tau}-\frac{u}{h}+\frac{E_i^n+E_{i+1}^n}{h^2}+K_i^n\right)C_{i,j+1}^n \\ -\frac{E_i^n}{h^2}C_{i-1,j+1}^n=\frac{1}{\tau}C_{i,j}^n \\ C_{0,j}^n=f(jh),\ C_{i,0}^n=\varphi(ih),\ C_{N+1,j}^n=C_{N,j}^n\end{cases} \tag{3}$$

The inverse calculation model about δE_i^n and δK_i^n can be written as follows:

$$\begin{cases}-\frac{\delta C_{i,j}^n}{\tau}-\delta C_{i-1,j+1}^n\frac{E_i^n}{h^2}+\delta C_{i,j+1}^n\left(\frac{1}{\tau}-\frac{u}{h}+\frac{E_i^n+E_{i+1}^n}{h^2}+K_i\right) \\ +\delta C_{i+1,j+1}^n\left(\frac{u}{h}-\frac{E_{i+1}^n}{h^2}\right)=\frac{\delta E_{i-1}^n}{h^2}(C_{i-1,j+1}^n-C_{i,j+1}^n) \\ +\frac{\delta E_i^n}{h^2}(C_{i,j+1}^n-C_{i+1,j+1}^n)-\delta K_i C_{i,j+1}^n \\ \delta C_{i,0}^n=\delta C_{0,j}^n=\delta C_{N,j}^n=\delta C_{N+1,j}^n=0 \\ (i=0,1,2,\ldots N, j=0,1,2,\ldots W)\end{cases} \tag{4}$$

The Green function $G_{i,j,p,q}$ is developed as follows:

$$\begin{cases}-\frac{E_i^n}{h^2}G_{i-1,j+1,p,q}+\left(\frac{1}{\tau}-\frac{u}{h}+\frac{E_i^nE_{i+1}^n}{h^2}+K_i^n\right)G_{i,j+1,p,q} \\ +\left(\frac{u}{h}-\frac{E_{i+1}^n}{h^2}\right)G_{i+1,j+1,p,q}-\frac{1}{\tau}G_{i,j,p,q}=G_{i,j,p,q} \\ (i=0,1,2,\ldots N, j=0,1,2,\ldots W)\end{cases} \tag{5}$$

where

$$G_{i,j,p,q}=\begin{cases}1(i=p,j=q).\\ 0(i\ne p,j\ne q)\end{cases} \tag{6}$$

Considering the difference equation and its boundary conditions, $G_{0,j,p,q-1}=G_{N,j,p,q-1}=0$. And the following expression can be got based on Equations (4)–(6):

$$\delta C_{N,q}^K=\sum_{i=1}^{N-1}\left\{\sum_{j=1}^{W-1}[G_{i,j,N,q}(C_{i-1,j+1}^n-C_{i,j+1}^n)+G_{i+1,j,N,q-1}(C_{i+1,j+1}^n-C_{i,j+1}^n)]\frac{\delta E_i^n}{h^2}-\sum_{j=1}^{W-1}G_{i,j,N,q}\cdot C_{i,j+1}^n\cdot\delta K_i^n\right\} \tag{7}$$

Equation (7) is the inverse equation for the forward flow direction, and those for other flow directions are similar to it, shown as follows.

Backward flow:

$$\delta C_{N,q}^K=\sum_{i=1}^{N-1}\left\{\sum_{j=1}^{W-1}[G_{i-1,j,N,q}(C_{i,j+1}^n-C_{i+1,j+1}^n)+G_{i,j,N,q-1}(C_{i,j+1}^n-C_{i+1,j+1}^n)]\frac{\delta E_i^n}{h^2}-\sum_{j=1}^{W-1}G_{i-1,j,N,q}\cdot C_{i+1,j+1}^n\cdot\delta K_i^n\right\} \tag{8}$$

Divergent flow:

$$\delta C_{N,q}^K=\sum_{i=1}^{N-1}\left\{\sum_{j=1}^{W-1}[G_{i,j,N,q}(C_{i,j+1}^n-C_{i-1,j+1}^n)+G_{i+1,j,N,q-1}(C_{i,j+1}^n-C_{i+1,j+1}^n)]\frac{\delta E_i^n}{h^2}+\sum_{j=1}^{W-1}G_{i,j,N,q}\cdot C_{i,j+1}^n\cdot\delta K_i^n\right\} \tag{9}$$

Convergent flow:

$$\delta C_{N,q}^K=\sum_{i=1}^{N-1}\left\{\sum_{j=1}^{W-1}[G_{i-1,j,N,q}(C_{i+1,j+1}^n-C_{i,j+1}^n)+G_{i,j,N,q-1}(C_{i+1,j+1}^n-C_{i,j+1}^n)]\frac{\delta E_i^n}{h^2}+\sum_{j=1}^{W-1}G_{i-1,j,N,q}\cdot C_{i+1,j+1}^n\cdot\delta K_i^n\right\} \tag{10}$$

Calibration for inverse calculation models

In this study Monte-Carlo Analysis (MCA) is used for assessing the sensitivity of the inverse calculation models. MCA

uses regional sensitivity analysis (RSA) to assess the sensitivity of model parameters (Soltani *et al.* 2010; Yoshiaki *et al.* 2010), where sensitivity is defined as the effect of changes in the parameters on the overall model performance (as indicated by an objective function). Sensitivity is only one of the essential requirements of an identifiable parameter. A parameter is termed identifiable if it is possible to determine its value with relative confidence within the feasible parameter space based on the model output produced. However, the values of sensitive parameters that produce a behavioral model output can be distributed over a range of the feasible parameter space and can change when they are estimated from different response modes (Maier *et al.* 2010). Hence MCA uses an identifiable analysis, which is based either on simple inspection of the 'dotty plots' of Monte-Carlo outputs for a given parameter, for example taken from the upper performance quantile, or from an automated analysis.

For water quality models, calibration and prediction periods are assessed using the Nash–Sutcliffe criteria (Telci *et al.* 2009):

$$R^2 = 1 - \frac{\sum_{i=1}^{N} (o_i - p_i)^2}{\sum_{i=1}^{N} (o_i - \bar{o})^2} \tag{11}$$

where o_i is the ith observed output variable, p_i is the ith predicted output variable, N is the number of observations and the over-bar denotes the mean for the period of evaluation. Note that the Nash–Sutcliffe criterion has a basic reliance on the square of the errors, which thus focuses on fitting peak values.

RESULTS AND DISCUSSION

The state of the flow

In this paper, based on the value of the flow rate in the tidal Foshan River, the state of the flow is divided into three grades: high flow, moderate flow and low flow. And the state is called

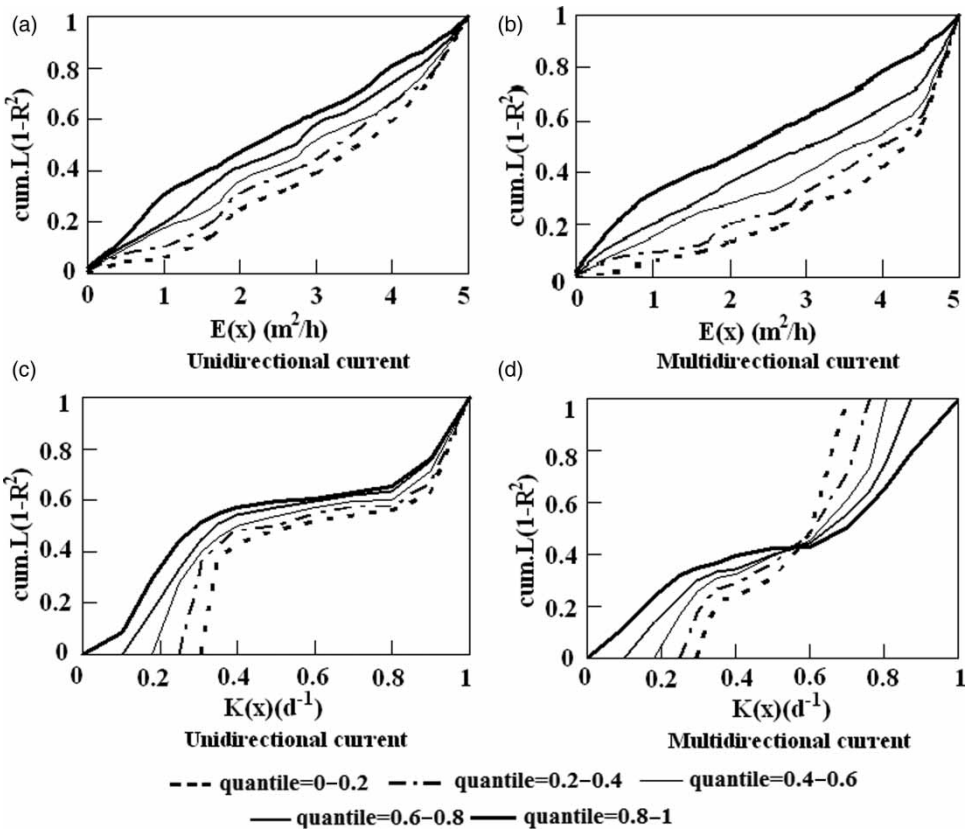

Figure 3 | Regional sensitivity plot of E(x) and K(x) in the inverse BOD model.

'high flow', 'moderate flow' and 'low flow' when the value of the flow rate is $>60\ m^3/s$, between $20\ m^3/s$ and $60\ m^3/s$ and $<20\ m^3/s$ respectively. According to the measurements, the high flow appears in the period 11 August to 13 November 2012, while the moderate flow happens during 26 March to 10 August 2012 and 13 November to 13 December 2012, and the low flow occurs 1 January to 25 March 2012 and 14 December to 30 December 2012. The inverse BOD models are developed on the basis of the different state of the flow.

Calibration of the model

Figure 3 shows a RSA of the behavior of the model parameters. The objective functions are then transformed into likelihood values (i.e. the chance of occurrence) split into five quantile groups, and the cumulative frequency distribution is calculated and plotted (Wagener *et al.* 2001). If the model performance is sensitive to a particular parameter there will be a large difference between the cumulative frequency distributions of the quantile groups. If the model performance is not sensitive to a particular parameter, given an a priori uniform distribution each group will plot on a straight line (Wagener *et al.* 2001). Five quantile groups are ranked from the highest to the lowest likelihood in Figure 3. The result shows that E(x) is more sensitive for the models of the multidirectional flows than those of the unidirectional flows. The similar conclusion can be drawn from the regional sensitivity plot of K(x). In addition, K(x) is more sensitive to the BOD models than E(x) under the same flow direction condition.

Application of inversed BOD models to the tidal Foshan River

As an example, the variations of flow rate and flow velocity with hours in Stn b, e, g and i on 25 June are studied. The results shows that the unidirectional flows tend to occur when flow rate is $>20\ m^3/s$ and flow velocity is >40 cm/s, and the multidirectional flows happen while flow rate is $<20\ m^3/s$ and flow velocity is <0.4 cm/s.

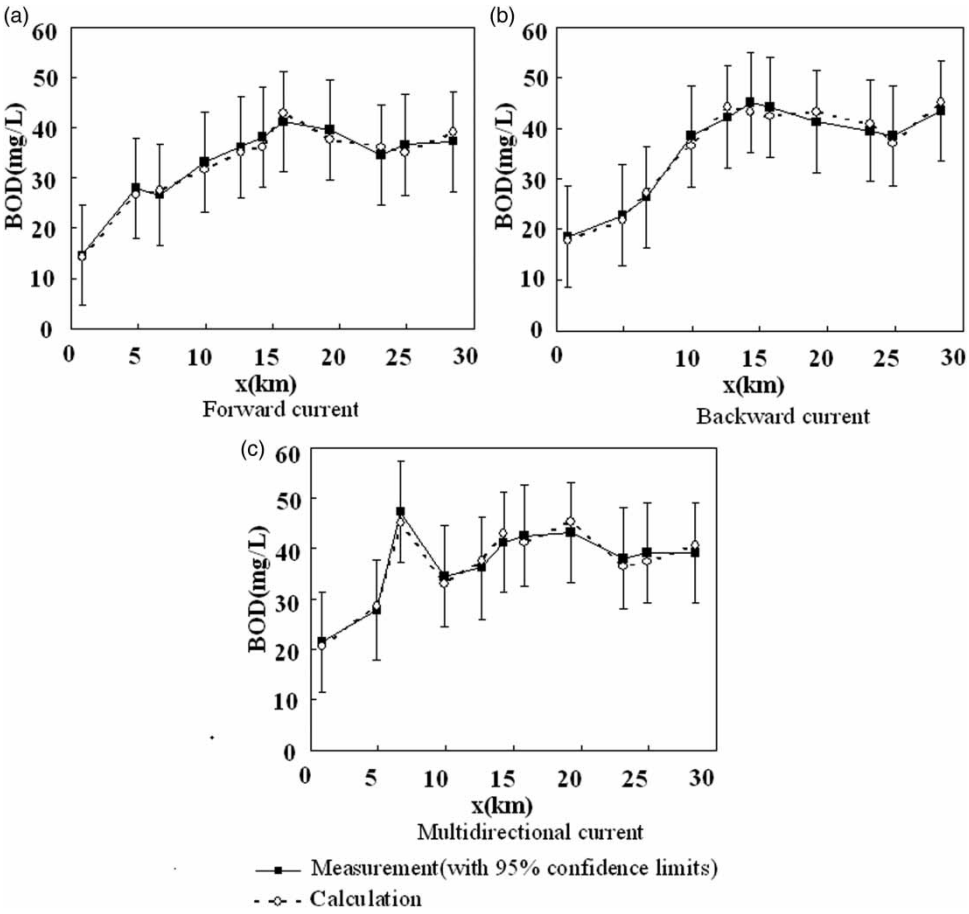

Figure 4 | Comparison of the calculated BOD with the measured BOD.

To examine the representativeness of the measured BOD obtained from central points of a cross-section, the measured BOD in the different sampling points of the cross-section of Stn b, e, g and i are measured as an example. The result shows that the range of the relative difference between the measured BOD from the central points and those from the other different points of each cross-section is −1.83 to 4.28%. Therefore the measured BOD from central points with 95% confidence limits can be a representative for all the measured ones from other points

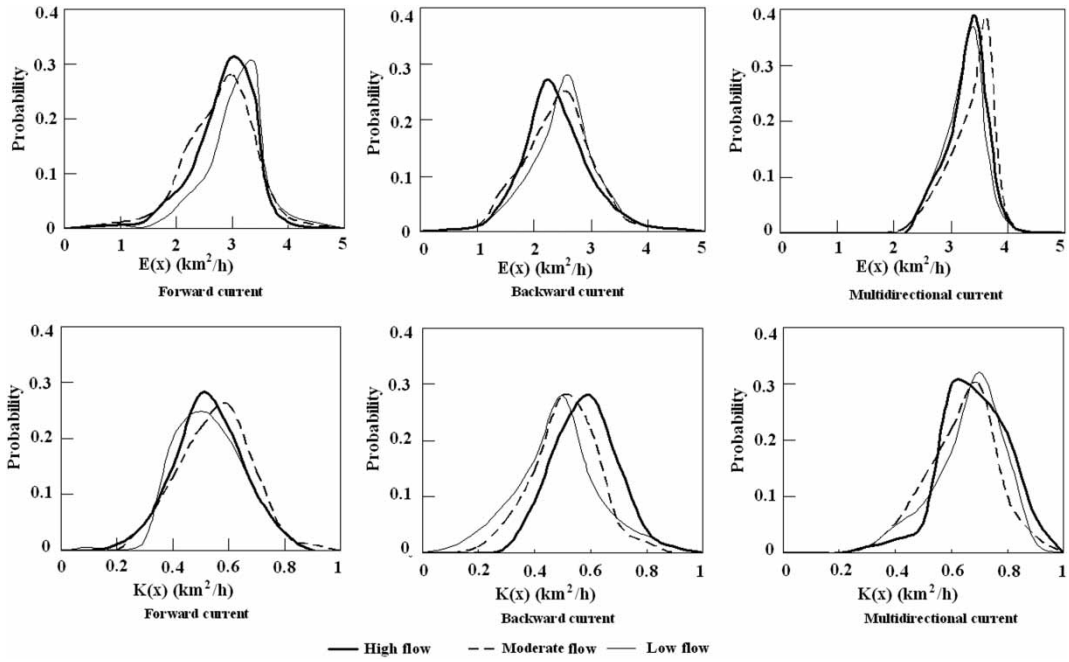

Figure 5 | Probability of E(x) in different flow directions.

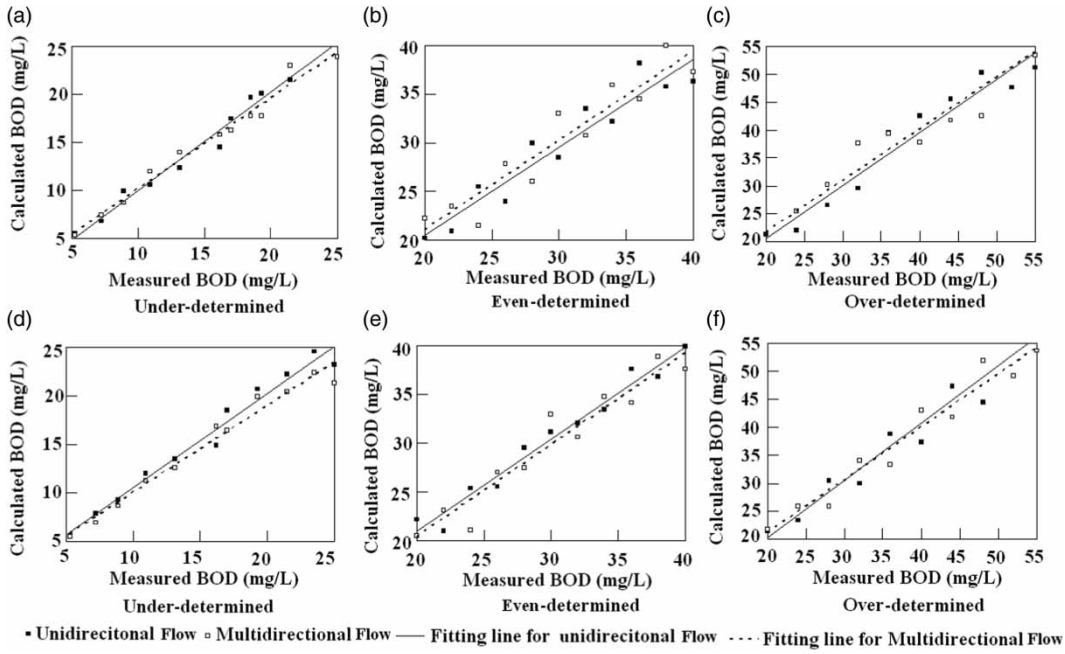

Figure 6 | Calculated BOD vs measured BOD with the different data sets ((a)–(c) for E(x), (d)–(f) for K(x)).

of the whole cross-section. Therefore in this work, the following measured BOD used for study are all from the central point of each cross-section.

Comparison of the inversely calculated BOD with the measured ones is shown in Figure 4. The minimum, maximum and average of relative difference in the forward flow are 1.65%, 2.63% and 2.15% respectively; the minimum, maximum and average one in the backward flow are 1.48%, 2.95% and 2.51% respectively; and the minimum, maximum and average one in the multidirectional flow are 2.17%, 3.19% and 2.66% respectively. Therefore the match between the inversely calculated BOD and the measured ones is satisfactory.

Further verification of the parameters of the models

To further verify the validity of the models, the performance of the models is studied under different data sets for the estimations of E(x) and K(x). Figure 5 shows the statistical probability of the calculated E(x) and K(x) in high flow, moderate flow and low flow. It can be concluded from Figure 5 that most of the values of E(x) and K(x) are within 3–4 km^2/h and 0.5–0.8 d^{-1} respectively. Therefore three data sets such as even-determined, over-determined, under-determined one are used, and in this paper the data set of E(x) is defined as 'under-determined', 'even-determined' and 'over-determined' measurement when the value of E(x) is $<3\ km^2/h$, 3–4 km^2/h and $>4\ km^2/h$ respectively. And the data set of K(x) is named as 'under-determined', 'even-determined' and 'over-determined' when the value of K(x) is $<0.5\ d^{-1}$, 0.5–0.8 d^{-1} and $>0.8\ d^{-1}$ respectively.

Figure 6 shows the values of measured BOD as a function of the calculated values from the models in the above three different data sets for E(x) and K(x) under different flow directions condition. The results show that all of the regression coefficients between the calculated and measured values are >0.96, and the ranges of relative differences between the calculated and measured ones are all <5.1%. Thereby the calculated results match the measured ones well. This indicates that the different data sets hardly affect the performance of the inversely calculated models under different flow directions condition.

CONCLUSION

The inverse calculations of longitudinal dispersion coefficient (E(x)) and BOD decay rate (K(x)) of the BOD models are developed based on time domain under different flow directions conditions for the tidal Foshan River and their steady solutions are established. The results demonstrate that the calculated values of BOD match the measured ones well and this match is affected scarcely by different data sets (over-determined, even-determined, under-determined) for the estimation of E(x) and K(x).

REFERENCES

Ani, E.-C., Wallis, S., Kraslawski, A. & Agachi, P. S. 2009 Development, calibration and evaluation of two mathematical models for pollutant transport in a small river. *Environmental Modelling & Software* **24** (10), 1139–1152.

Atkinson, S. F., Johnson, D. R., Venables, B. J., Slye, J. L., Kennedy, J. R., Dyer, S. D., Price, B. B., Ciarlo, M., Stanton, K., Sanderson, H. & Nielsen, A. 2009 Use of watershed factors to predict consumer surfactant risk, water quality, and habitat quality in the upper Trinity River, Texas. *Science of The Total Environment* **407** (13), 4028–4037.

Beck, J. V., Blackwell, B. & Haji-Sheikh, A. 1996 Comparison of some inverse heat conduction methods using experimental data. *International Journal of Heat and Mass Transfer* **39** (17), 36–49.

Denman, K. L. & Powell, T. M. 1984 Effects of physical processes on planktonic ecosystems in the coastal ocean. *Oceanography and Marine Biology* **22** (4), 125–168.

Er, L., Yuehua, F. & Man, L. 2009 *The Evolution and Models of the Foshan River Estuary*. Huazhong University of Science and Technology Press, Wuhan, China, pp. 33–72 (in Chinese).

Erturk, A., Gurel, M., Ekdal, A., Tavsan, C., Ugurluoglu, A., Seker, D. Z., Tanik, A. & Ozturk, I. 2010 Water quality assessment and meta model development in Melen watershed – Turkey. *Journal of Environmental Management* **91** (7), 1526–1545.

Franceschini, S. & Tsai, C. W. 2010 Assessment of uncertainty sources in water quality modeling in the Niagara River. *Advances in Water Resources* **33** (4), 493–503.

Freni, G., Mannina, G. & Viviani, G. 2011 Assessment of the integrated urban water quality model complexity through identifiability analysis. *Water Research* **45** (1), 37–50.

Ghermandi, A., Vandenberghe, V., Benedetti, L., Bauwens, W. & Vanrolleghem, P. A. 2009 Model-based assessment of shading effect by riparian vegetation on river water quality. *Ecological Engineering* **35** (1), 92–104.

Maier, H. R., Jain, A., Dandy, G. C. & Sudheer, K. P. 2010 Methods used for the development of neural networks for the prediction of water resource variables in river systems: flow status and future directions. *Environmental Modelling & Software* **25** (8), 891–909.

Mannina, G. & Viviani, G. 2010 Water quality modelling for ephemeral rivers: Model development and parameter assessment. *Journal of Hydrology* **393** (3), 186–196.

Paredes, J., Andreu, J. & Solera, A. 2010 A decision support system for water quality issues in the Manzanares River (Madrid, Spain). *Science of The Total Environment* **408** (12), 2576–2589.

Soltani, F., Kerachian, R. & Shirangic, E. 2010 Developing operating rules for reservoirs considering the water quality issues: application of ANFIS-based surrogate models. *Expert Systems with Applications* **37** (9), 6639–6645.

Svejkovsky, J., Nezlin, N. P., Mustain, N. M. & Kum, J. B. 2010 Tracking stormwater discharge plumes and water quality of the Tijuana River with multispectral aerial imagery. Estuarine. *Coastal and Shelf Science* **87** (3), 387–398.

Telci, I. T., Nam, K., Guan, J. & Aral, M. M. 2009 Optimal water quality monitoring network design for river systems. *Journal of Environmental Management* **90** (10), 2987–2998.

Wagener, T., Boyle, D. P., Lees, M. J., Wheater, H. S., Gupta, H. V. & Sorooshian, S. 2001 A framework for the development and application of hydrological models. *Hydrology and Earth System Sciences* **5** (1), 100–140.

Xiangying, Z., Er, L. & Yuehua, F. 2012 *Researches on the Polluted Material of the Tidal Foshan River and its Tributary*. Press of Environment Protection Research Institute of Foshan, Foshan, China, pp. 30–357 (in Chinese).

Yin, K., Harrison, P. J., Pond, S. & Beamish, R. J. 1995 Entrainment of nitrate in the Fraser River plume and its biological implications. II. Effects of spring vs neap tides and river discharge. *Estuarine Coastal and Shelf Science* **40** (1), 529–544.

Yoshiaki, T., Masato, F., Yasuo, M., Kouki, M. & Minoru, Y. 2010 Natural purification effects in the river in consideration with domestic wastewater pollutant discharge reduction effects. *Journal of Environmental Sciences* **22** (6), 892–897.

Zheng, Y. & Gore, J. P. 2005 Measurements and inverse calculations of spectral radiation intensities of a turbulent ethylene/air jet flame. *Proceedings of the Combustion Institute* **30** (5), 727–734.

First received 16 August 2013; accepted in revised form 25 March 2014. Available online 16 April 2014